Characterization of Pyrogenic Black Carbon by Desorption Atmospheric Pressure Photoionization Fourier Transform Ion Cyclotron Resonance Mass Spectrometry

ARTICLE *in* ANALYTICAL CHEMISTRY · FEBRUARY 2012

Impact Factor: 5.64 · DOI: 10.1021/ac202166x · Source: PubMed

7 AUTHORS, INCLUDING:

David C Podgorski
Florida State University
26 PUBLICATIONS **297** CITATIONS
SEE PROFILE

Amy M. Mckenna
Florida State University
54 PUBLICATIONS **980** CITATIONS
SEE PROFILE

William T Cooper
Florida State University
99 PUBLICATIONS **1,829** CITATIONS
SEE PROFILE

analytical chemistry

Article

pubs.acs.org/ac

Characterization of Pyrogenic Black Carbon by Desorption Atmospheric Pressure Photoionization Fourier Transform Ion Cyclotron Resonance Mass Spectrometry

David C. Podgorski,[†] Rasha Hamdan,[†] Amy M. McKenna,[‡] Leonard Nyadong,[‡] Ryan P. Rodgers,[†,‡] Alan G. Marshall,[†,‡] and William T. Cooper*[,†]

[†]Department of Chemistry and Biochemistry, Florida State University, Tallahassee, Florida 32306-4390, United States

[‡]National High Magnetic Field Laboratory, Florida State University, 1800 East Paul Dirac Drive, Tallahassee, Florida 32310-4005, United States

ABSTRACT: We present a new method for molecular characterization of intact biochar directly, without sample preparation or pretreatment, on the basis of desorption atmospheric pressure photoionization (DAPPI) coupled to Fourier transform ion cyclotron resonance (FTICR) mass spectrometry. Conventional ionization methods (e.g., electrospray or atmospheric pressure photoionization) for characterization of natural organic matter have limited utility for the characterization of chars due to incomplete solubility in common solvents. Therefore, direct ionization techniques that do not require sample dissolution prior to analysis are ideal. Here, we apply DAPPI FTICR mass spectrometry to enable the first molecular characterization of uncharred parent oak biomass and after combustion (250 °C) or pyrolysis (400 °C). Parent oak is primarily composed of cellulose-, lignin-, and resin-like compounds. Oak combusted at 250 °C contains condensed aromatic compounds with low H/C and O/C ratios while retaining compounds with high H/C and O/C ratios. The bimodal distribution of aromatic and aliphatic compounds observed in the combusted oak sample is attributed to incomplete thermal degradation of lignin and hemicellulose. Pyrolyzed oak constituents exhibit lower H/C and O/C ratios: approximately three-quarters of the identified species are aromatic. DAPPI FTICR MS results agree with bulk elemental composition as well as functional group distributions determined by elemental analysis and solid state ^{13}C NMR spectroscopy. Complete molecular characterization of biomass upon thermal transformation may provide insight into the biogeochemical cycles of biochar and future renewable energy sources, particularly for samples currently limited by solubility, separation, and sample preparation.

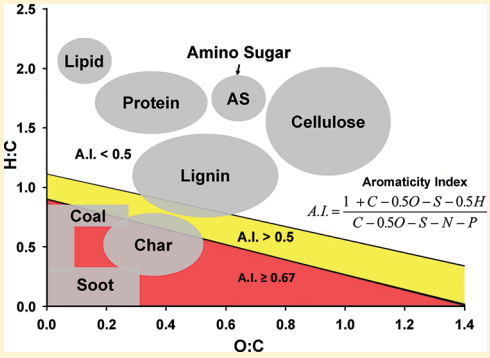

Combustion products from thermally degraded vegetation (i.e., "black carbon" or BC) range from slightly charred biomass (biochar) to charcoal, soot, and graphite according to the degree of thermal degradation. Terrestrial soil and sediments contain BC, and groundwater runoff transports BC to marine sediments.[1] Although BC is a heterogeneous mixture with a wide range of chemical and physical properties, most BC remains in the environment and is resistant to biological or chemical degradation.[2−4] Characterization and quantitation of BC in the global carbon budget is of recent interest because BC may act as a significant carbon sink, moving carbon from the relatively rapid bioatmospheric cycle to the slower sedimentary cycle.[5−7]

Contrary to previous reports that all BC is inert, Baldock and Smernick reported on the presence of reactive BC and concluded that the degree of subsequent degradation depends on the extent of thermal alteration of certain organic components in the postfire residue.[8] Degradation of BC occurs through two main processes: microbial and photochemical.[8−10] Shneour found that 2% of artificial graphite is oxidized in nonsterile soils.[11] Scott et al. and Hofrichter et al. identified several fungi able to decompose low-grade coals.[12,13] They provided evidence that BC undergoes some degradation in the environment but on a time scale ranging from a few to thousands of years.[10,14−16]

Previous characterization of char has been based on nuclear magnetic resonance (NMR) spectroscopy,[17−19] which provides structural and bulk property measurements, but does not identify molecular rearrangements that occur upon release into the environment. Fourier transform ion cyclotron resonance (FTICR) mass spectrometry has been routinely applied to characterize complex organic mixtures due to the high mass accuracy (<200 ppb) and ultrahigh resolution ($m/\Delta m_{50\%}$ = 400 000 at m/z 400) required for accurate elemental composition assignments.[20,21] Previous molecular characterizations of BC by FTICR MS have included an examination of the composition of water-soluble components of charcoal extracted from the water solvent by hydrophobic cartridges.[22] Several other studies identified the changes in elemental

Received: August 16, 2011
Accepted: December 23, 2011
Published: December 23, 2011

   dx.doi.org/10.1021/ac202166x | *Anal. Chem.* 2012, 84, 1281−1287

composition of the water-soluble fraction after it enters and is transported through an aquatic environment.[23−25] However, we are unaware of any reports of ultrahigh resolution FTICR mass spectral analysis of solid biochars. Here, we present the direct ionization and molecular characterization of a solid oak and oak biochars before and after combustion and pyrolysis.

Direct ionization techniques enable the rapid analysis of solid samples with little or no sample pretreatment by placing them in an atmospheric pressure chamber that interfaces to the mass spectrometer inlet. Thermal desorption is the oldest of atmospheric pressure surface sampling techniques and is often combined with chemical ionization to produce gas phase ions from solid samples suitable for mass spectrometric analysis.[26] However, Chen et al.[27] demonstrated that certain organic salts could be thermally desorbed as ions under ambient conditions. Laser desorption is also popular for sampling surfaces under ambient conditions and, like thermal methods, is most commonly combined with chemical ionization by means of a corona discharge.[28] Recently, electrospray-assisted laser desorption/ionization (ELDI) has been receiving increasing attention.[29,30]

Included in this class of direct ionization methods for solids are the increasingly popular desorption electrospray ionization (DESI)[31] and direct analysis in real time (DART) based on a corona discharge.[32] Both of these can be considered "ambient" ionization techniques.[33] However, DESI and DART are limited to the analysis of polar analytes. Here, we present the first coupling of desorption atmospheric pressure photoionization (DAPPI) to FTICR MS, thereby taking advantage of all of the inherent benefits of APPI to enable analysis of compounds spanning a wide range of polarity.[34] DAPPI was first introduced in 2007, and detailed mechanistic characterization has been reported.[35,36] In DAPPI, a heated nebulizer produces a plume of hot gas/solvent that is directed to the surface of a sample to desorb neutral analyte molecules into the gas phase.[35] The desorbed analytes are then ionized by the same mechanisms as with APPI.[36] APPI can ionize an analyte molecule directly, resulting in loss of an electron to generate a molecular radical cation, $M^{+\bullet}$. For such direct photoionization to occur, the energy of the photon must be greater than the ionization energy of the analyte. However, the radiation output of a conventional APPI krypton UV lamp is normally too low for efficient direct photoionization.[36] As a result, Bruins et al. developed dopant-assisted APPI[36] in which an excess of photoionizable reagent (dopant, D) provides $D^{+\bullet}$ ions that can easily react with analyte, M, by proton transfer or charge exchange to generate $M^{+\bullet}$ or $[M + H]^+$ ions. Dopant-assisted APPI can increase ionization efficiency by 2−3 orders of magnitude.[34] The choice of dopant for DAPPI determines the type/distribution of analyte ions generated: $[M + H]^+$ vs $M^{+\bullet}$ or $[M - H]^-$ vs $M^{-\bullet}$. It should be selected to increase ionization efficiency for compounds of interest.[37] DAPPI has been applied to the analysis of pharmaceutical tablets,[35] illicit drugs,[38] polycyclic aromatic hydrocarbons in soil,[39] pesticides on produce,[39] and MS imaging of biological tissue.[40]

Here, for the first time, we present the molecular composition of a solid oak sample, as well as the composition of solid oak biochars after combustion at 250 °C and pyrolysis at 400 °C (henceforth denoted as parent oak, oak 250, and oak 400) by DAPPI FTICR MS without sample preparation or preseparation. Our method provides an experimental framework for enhanced molecular level characterization of biochar and its reactivity in the environment. A potential limitation of DAPPI is that neutrals are desorbed from the surface of a sample. If a sample is not homogeneous, DAPPI may not provide information about the entire sample. In this work, we have included data from solid-state NMR and elemental analysis. The data obtained from these bulk analyses were used to corroborate the molecular level information obtained by DAPPI FTICR MS.

EXPERIMENTAL SECTION

Samples. *Quercus laurifolia* (laurel oak) without bark was dried thoroughly and cut into 1 × 1 × 5 cm pieces. Portions of approximately 1.5 g were loosely wrapped in foil and baked in a 0.04 m^3 combustion oven or heated in a pyrolyzer (5.5 cm diameter × 50 cm length pipe). In the pyrolysis experiment, N_2 gas flowed over the sample at a rate of approximately 2.3 oven volumes min^{-1}. The heating rate was 10−12 °C min^{-1}, and peak temperature hold time (250 and 400 °C) was 3 h for combustion and pyrolysis.

DAPPI Source. A ThermoFisher IonMaxx ion source equipped with a krypton UV lamp was used for all linear ion trap MS experiments, and a modified ThermoFisher LCQ APPI (ThermoFisher Corp., Bremen, Germany) source was used for all 9.4 T FTICR MS experiments.[41] Parent and charred biomass were held ∼1 mm from the exit of the heated ceramic nebulization tube by tweezers. The sample was 10 mm from the MS inlet. Gas-phase neutrals were produced through thermal and chemical desorption. Nitrogen was used as nebulizer gas at 100 psi with toluene as dopant at a flow rate of 50 μL min^{-1}. The temperature of the heated nebulizer gas/solvent plume ranged from 100 to 500 °C depending upon the sample. The temperature of the MS inlet capillary was 200 °C, and the tube lens voltage was set at −35 V.

Linear Ion Trap Mass Spectrometry. Molecular weight distributions were determined with a ThermoFisher linear ion trap (LTQ ThermoFisher Corp., Bremen, Germany) mass spectrometer. LTQ mass spectra were obtained for molecular weight determination and for desorption temperature optimization based on signal intensity measurements across a temperature range of 100−500 °C. Negative ion mass spectra were acquired with automatic gain control.[42] Data were acquired with Xcalibur verson 2.0 software at a maximum injection period of 2000 ms and a scan speed of 3 scans/spectrum. Fifty scans were acquired for each sample. For parent oak, 100 °C produced the highest signal intensity, while the highest intensities for oak 250 and oak 400 were at 200 and 350 °C, respectively (Figure 1).

FTICR Mass Spectrometry. FTICR mass spectra were acquired with a passively shielded 9.4 T superconducting magnet (Oxford Instruments, Abingdon, Oxfordshire OX13 5QX United Kingdom) located at the National High Magnetic Field Laboratory in Tallahassee, Florida.[43] Time-domain transient signals were collected and processed by a modular ICR data acquisition system.[44] Negative ions were accumulated (50−500 ms) externally[45] in the second rf-only octopole and collisionally cooled with helium prior to transfer through an rf-only octopole to a seven segment open cylindrical cell with capacitively coupled excitation electrodes similar to the configuration of Tolmachev et al.[46,47] Chirp excitation (∼700−90 kHz at a sweep rate of 50 Hz μs^{-1} and 360 V_{p-p} amplitude) accelerated the ions to a detectable cyclotron radius. Approximately 10−20 time-domain acquisitions were coadded, Hanning-apodized, and zero-filled once prior to fast Fourier transform and magnitude calculation. Frequency was converted

dx.doi.org/10.1021/ac202166x | Anal. Chem. 2012, 84, 1281−1287

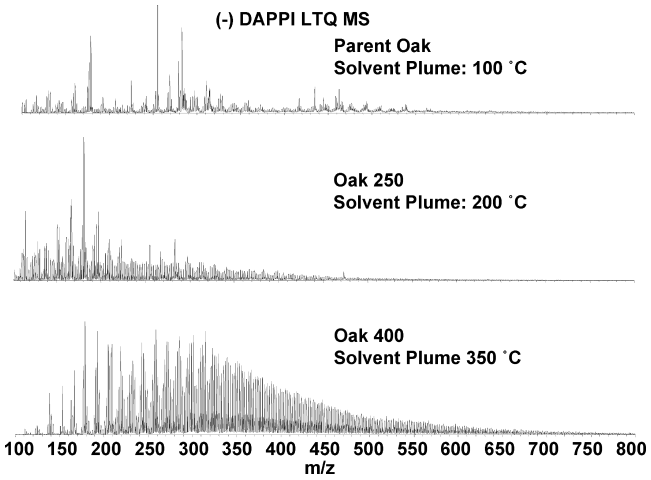

Figure 1. Broadband (−) DAPPI LTQ mass spectra of the parent oak, oak combusted at 250 °C, and oak pyrolyzed at 400 °C. The optimum solvent plume temperature was determined for each sample. Top: The mass spectrum is typical of fresh, labile organic biomass. Middle and Bottom: These mass spectra exhibit a broad pseudo-Gaussian distribution as the biomass is thermally degraded.

to m/z by the quadrupolar electric trapping potential approximation.[48,49] Spectra were internally calibrated from extended homologous alkylation series (compounds that differ in elemental composition by integer multiples of CH_2) of high relative abundance.

Data Analysis. Every peak in the mass spectra for which a unique molecular formula could be assigned was sorted by elemental composition (C, H, O). Elemental H/C and O/C ratios were then calculated, and the formulas were projected onto a van Krevelen diagram, namely, a plot of H/C vs O/C ratio (Figure 2).[16,50,51] In such a diagram, compounds with

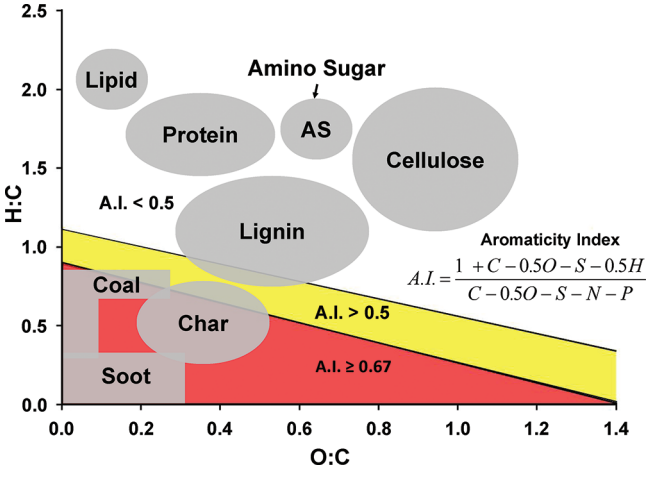

Figure 2. van Krevelen diagram of elemental H/C vs O/C ratios. Molecular formulas with similar chemical characteristics tend to fall within specific regions. van Krevelen plots of different samples may be compared to determine changes in chemical composition. Formulas with aromaticity index (AI) values >0.5 are considered aromatic, and those with AI > 0.67 are condensed aromatic.

similar chemical properties tend to locate in specific regions. The double bond equivalents parameter (DBE = number of rings plus double bonds to carbon) measures hydrogen deficiency and is calculated from the elemental composition, $C_cH_hN_nO_oS_s$ ($DBE = c - h/2 + n/2 + 1$) as determined by FTICR mass spectrometry.[24,52] DBE and oxygen class are plotted as a function of percent relative abundance to illustrate compositional changes in aromaticity and oxygen number under different thermal conditions. Each elemental formula was assigned a modified aromaticity index (AI) based on the system proposed by Koch and Dittmar.[23] Here, formulas are classified as nonaromatic (AI < 0.5), aromatic (AI > 0.5), and condensed aromatic (AI ≥ 0.67) (Figure 2). It is important to note that this AI is a conservative parameter used to identify compounds that are unequivocally aromatic based on low H/C ratios. Some uncertainty is involved in classifying an individual molecular formula as aromatic based on AI alone. Specifically, non-aromatic carboxyl-rich aliphatic acids (CRAM) and aromatic lignin can have similar molecular formulas and therefore occupy the same compositional space in a van Krevelen diagram.[53] For example, some aromatic monomeric components of lignin may be identified as aromatic based on AI > 0.5, e.g., vanillin (0.54), vanillic acid (0.5), *p*-coumaric acid (0.6), and ferulic acid (0.5), whereas other lignin monomers may have AI < 0.5, e.g., acetovanillone (0.47), syringaldehyde (0.43), acetosyringone (0.38), and syringic acid (0.38). Thus, highly substituted aromatics, like lignin monomers, may not be identified as aromatic based on the AI parameter. However, AI along with van Krevelen diagrams are efficient tools for visualizing relative changes in the elemental composition of organic materials resulting from thermal degradation.

Nuclear Magnetic Resonance Spectroscopy. Solid-state ^{13}C NMR spectra were obtained with a widebore Varian Inova 500 MHz spectrometer operated at 125 MHz. Each sample (~100 mg) was packed in a 4 mm O.D. zirconium rotor and sealed with KEL-F caps. A small amount of internal standard, sodium trimethyl silanolate (Na-TMS), was added to the rotor but physically separated from the sample. Na-TMS appears as a sharp resonance at ~0 ppm and is well-resolved from all sample peaks. Spectra were acquired by use of ramped-cross-polarization (CP) and magic angle spinning (MAS) at 14 kHz. Ramped CP overcomes the inefficiency of cross-polarization between ^1H and ^{13}C in high-speed MAS and decreases in sensitivity from magnetic field inhomogeneity.[54] A 3 s pulse delay five times longer than the longest ^1H spin lattice relaxation time minimizes saturation effects. Twenty thousand free induction decays were summed for each sample, zero-filled once, and processed with 50 Hz Lorentzian line broadening. Functional group distributions were determined by integrating over defined chemical shift regions: 0−50 ppm (alkyl C), 50−60 ppm (N-alkyl and methoxy), 60−110 ppm (O-alkyl C including carbohydrates), 110−160 ppm (aromatic C), and 160−220 ppm (carbonyl C in carboxylic acids, esters, amides, ketones, and aldehydes).

Elemental Analysis. Bulk elemental analyses were performed with a ThermoFinnigan (Milan, Italy) Elemental Analyzer (Flash EA 1112) for total C, H, N, S, and O content. Each sample (~1−2 mg) was weighed into a silver container for oxygen determination (CE Elantech, Inc., Lakewood, NJ) or a tin container (ThermoFinnigan Italia, Milan, Italy) for CHNS analysis, crushed into a sphere, placed in an autosampler, and analyzed in quadruplicate. Calibration is based on elemental analysis of sulfanilamide (Thermo Electron S.p.A., Milan, Italy, CAS# 63-74-1; C: ±0.210; H: ±0.030; O: ±0.0834), and all quadruplicate runs included a separate, independent standard not used in the initial calibration.

dx.doi.org/10.1021/ac202166x | *Anal. Chem.* 2012, 84, 1281−1287

RESULTS AND DISCUSSION

Molecular Characterization of Biochar. *Parent Oak.* Figure 3 (top) shows the van Krevelen diagram for molecular

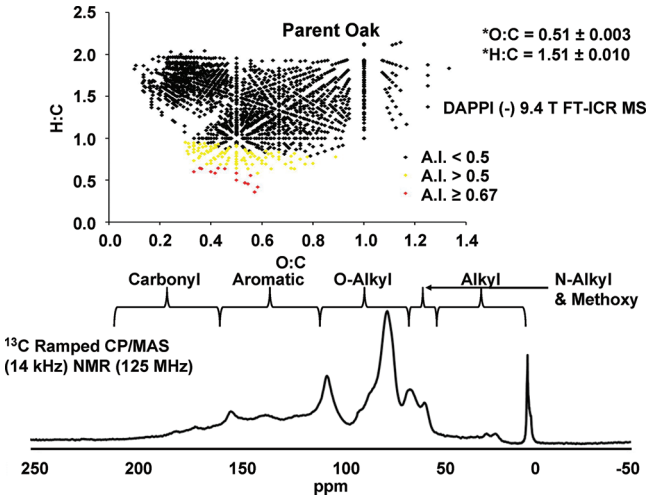

Figure 3. (Top) van Krevelen diagram for the elemental compositions assigned to parent oak by DAPPI FTICR MS. The molecular formulas fall within regions typical of wood components, i.e., lignin, resin, and cellulose. A few formulas are associated with aromatic compounds, i.e., A.I. > 0.5. (Bottom) NMR spectrum for parent oak. The spectrum is dominated by the O-alkyl peak, 60−110 ppm, with only minor contribution from the aromatic peak, 110−160 ppm. The sharp peak at 0 ppm is the internal standard Na-TMS. (*bulk O/C and H/C ratios determined by elemental analysis.)

formulas detected for parent oak determined by DAPPI FTICR MS. Most of assigned molecular formulas have high H/C and O/C with AI < 0.5, the threshold for aromatic structures based on the Koch/Dittmar method.[23] Although few formulas exhibit AI > 0.5, suggesting that aromatic compounds constitute a minor fraction of the overall composition of the parent oak, a significant number of formulas nevertheless fall within the lignin-like region of the VK diagram, a result consistent with the NMR data. Clearly, the AI parameter does not identify many of the highly substituted phenols that are the monomeric components of lignin.

Most molecular formulas lie in regions associated with cellulose-, aminosugar-, lignin-, and protein-like compounds. Wood is composed of ∼50% cellulose and ∼30% lignin; therefore, a large contribution of formulas with cellulose- and lignin-like molecular formulas is expected.[55] Formulas identified as protein-like are most likely not actually proteins, since the nitrogen content of this oak material is quite low (0.15%) and the C/N ratio is very high (∼350). Zhong et al.[56] analyzed a pyridine extract of a wood resin by ESI FTICR MS and noted that most of the formulas identified were located in this same protein-like region. The high concentration of formulas in the protein-like region of the VK diagram of parent oak thus most likely represents such resin-like components.

To determine if DAPPI ionization is representative of the native sample, molecular compositions obtained by FTICR MS were compared to ^{13}C NMR results. Figure 3 (bottom) shows the RAMP CP ^{13}C NMR spectrum for the parent oak. The predominant peaks in the NMR spectrum of parent oak are between 60 and 110 ppm, the region associated with O-alkyl functionality. O-Alkyl compounds have high O/C ratio, in accord with DAPPI FTICR MS and bulk elemental analysis. Only a minor contribution is observed in the aromatic region of the NMR spectrum (110−160 ppm), consistent with MS results. The average O/C and H/C ratios of parent oak obtained by elemental analysis are 0.51 ± 0.003 and 1.51 ± 0.010, which are in agreement with the abundance weighted average O/C and H/C of 0.55 and 1.43 obtained by DAPPI FTICR MS. High H/C and O/C ratios of the parent material are consistent with prior ^{13}C NMR spectra of higher-plant biomass which are dominated by O-alkyl species, a reflection of the dominance of cellulose.[8,51,57]

Oak Combusted at 250 °C. A shift to formulas of lower H/C is evident in the van Krevelen diagrams of oak 250 (Figure 4

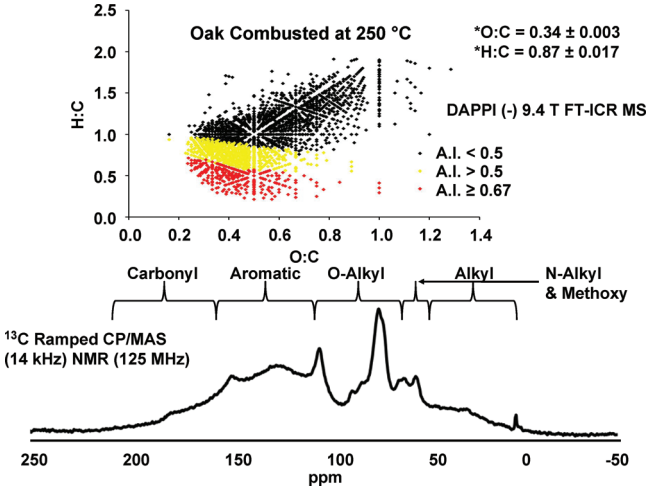

Figure 4. (Top) van Krevelen diagram for the elemental compositions assigned to oak combusted at 250 °C by DAPPI FTICR MS. Molecular formulas characteristic of aromatic and condensed aromatics, i.e., AI > 0.5 and AI ≥ 0.67, are formed relative to the parent oak. Although the elemental compositions associated with resins disappear relative to parent oak, compounds with high O/C and H/C associated with cellulose remain. (Bottom) NMR spectrum of oak 250, showing a decrease in the O-alkyl peak and increase in the aromatic peak relative to the parent oak. The sharp peak at 0 ppm is the internal standard Na-TMS. (*bulk O/C and H/C ratios determined by elemental analysis.)

(top)). Most formulas in the region associated with resin-like compounds are lost, and a significant number of formulas with AI > 0.5 are formed. The appearance of aromatic and condensed aromatic structures after the combustion of biomass is expected because degradation followed by dehydration of cellulose from 200 to 300 °C is responsible for the accumulation of new aryl compounds.[58] Furthermore, molecular formulas with AI ≥ 0.67, i.e., condensed aromatics, are observed for oak 250. Although elemental formulas associated with resin-like compounds disappear after combustion at 250 °C relative to the parent oak, formulas with H/C and O/C associated with cellulose-like compounds remain. Elemental compositions with high H/C and O/C ratios in oak 250 may indicate multiple processes. First, the elemental compositions that remain in that region suggest that a fraction of cellulose resists degradation by combustion at 250 °C and remains mostly intact. Second, those compounds may be byproducts of incomplete combustion.

RAMP CP ^{13}C NMR data (Figure 4 (bottom)) indicate a relative decrease in the O-alkyl signal and a relative increase in the aromatic region of the NMR spectrum of oak 250 relative

dx.doi.org/10.1021/ac202166x | Anal. Chem. 2012, 84, 1281−1287

to the parent oak. From the van Krevelen diagram, it is clear that some of the compounds with high H/C and O/C ratio are removed after combustion. The formation of aromatic compounds after combustion is confirmed by the relative increase in the aromatic peak in the NMR spectrum. Finally, the average O/C and H/C ratios for oak 250 obtained by bulk elemental analysis are 0.34 ± 0.003 and 0.87 ± 0.017, and the abundance weighted average O/C and H/C ratios obtained by DAPPI FTICR MS are 0.44 and 0.93, suggesting that oak 250 consists primarily of aromatic-like compounds. However, DAPPI FTMS enables the simultaneous identification of the aromatic compounds and the high H/C and O/C compounds that are not discernible by bulk elemental analysis.

Oak Pyrolyzed at 400 °C. A van Krevelen diagram from FTICR MS data for oak pyrolyzed at 400 °C shows a marked increase in the number of formulas with AI values >0.5, consistent with aromatic and condensed aromatic compounds (Figure 5 (top)). Molecular formulas exhibit lower O/C and H/C relative to the parent oak and oak 250. A complete loss of elemental compositions associated with cellulose-like compounds is observed in the oak 400 char. Significant depolymerization of cellulose occurs from 300 to 350 °C; therefore, a loss of most of the cellulose-like compounds in oak 400 is consistent with prior reports.[59]

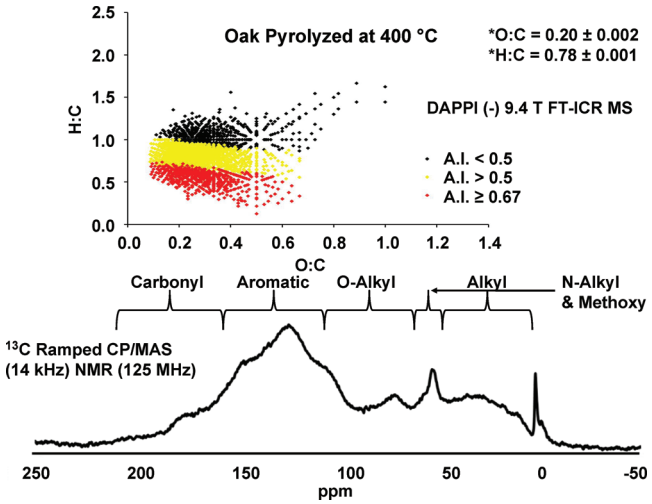

Figure 5. (Top) van Krevelen diagram of the molecular formulas assigned to oak pyrolyzed at 400 °C. Molecular formulas exhibit lower O/C and H/C ratios relative to parent oak and oak 250 due to depolymeriztion of cellulose and dehydration and deacetylation of lignin and cellulose. Approximately half of the elemental compositions assigned to oak 400 have an AI > 0.5. (Bottom) NMR spectrum of oak 400. The spectrum is dominated by the aromatic peak. There is almost no O-alkyl contribution relative to the parent oak and oak 250. The sharp peak at 0 ppm is the internal standard Na-TMS. (*denotes bulk O/C and H/C ratios determined by elemental analysis.)

The DAPPI FTICR MS data for oak 400 again agree with RAMP CP ^{13}C NMR data (Figure 5 (bottom)). Here, the predominant NMR peak is in the aromatic region. The peak in the O-alkyl region of the pyrolyzed oak NMR spectrum is reduced in magnitude so as to be barely resolvable relative to the parent oak and oak 250. Only a few of the compounds with high H/C and O/C ratios remain. Moreover, the van Krevelen diagram for oak 400 identifies more than 75% of the assigned formulas as aromatic or condensed aromatic. Finally, the average O/C and H/C ratios for oak 400 from bulk elemental analysis are 0.20 ± 0.002 and 0.78 ± 0.001, and the abundance weighted average O/C and H/C ratios obtained by DAPPI FTICR MS are 0.27 and 0.81. Thus, the bulk elemental analysis reflects the predominance of aromatic compounds in oak 400 and agrees with the formulas plotted in the van Krevelen diagram.

DBE Distribution. Figure 6 shows DBE distributions for all assigned elemental compositions for negative DAPPI ions from parent oak, oak 250, and oak 400. Parent oak has relatively lower DBE than oak 250 and 400. Its DBE classes range from DBE 2 to 14 with the most abundant classes from DBE 3 to 6. The high relative abundance of classes with low DBE is expected for parent material dominated by O-alkyl functionality and high O/C and H/C species.

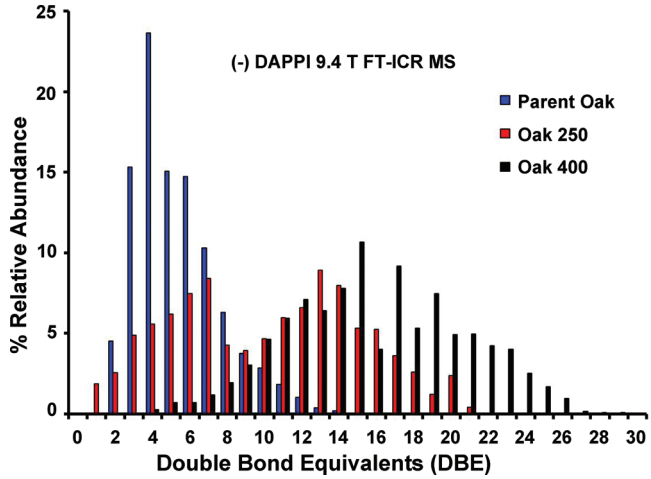

Figure 6. Double bond equivalents (DBE) relative abundance distribution for parent oak, oak 250, and oak 400. The parent oak has a relatively narrow range centered at low DBE, whereas oak 250 exhibits a bimodal distribution. Oak 400 is characterized by elemental compositions with relatively high DBE, the result of further thermal degradation of lignin and cellulose.

The DBE distribution for oak 250 is bimodal, ranging from DBE 1 to 21, with maxima at DBE 7 and 13. The first distribution is slightly higher in DBE than that for the parent oak, and the second distribution is slightly lower than that for oak 400. The DBE distributions are consistent with the van Krevelen plots. Elemental compositions with relatively high H/C and O/C correspond to the low DBE maximum and are associated with compounds that are either partially oxidized or not thermally degraded. The higher DBE maximum is associated with the species of AI > 0.5 that are formed after combustion.

The DBE distribution for oak 400 is dramatically different from that for the parent oak. High DBE values likely result from cleavage of aliphatic chains from aromatic rings, with an onset at approximately 300 °C. Furthermore, high DBE in addition to lower O/C and H/C for oak 400 could result from loss of acetic acid (e.g., the deacetylation of hemicellulose at 200−300 °C). Although the contribution from thermally unmodified lignin- and cellulose-like compounds make it unclear, deacetylation of hemicellulose may also explain the shift to lower DBE of oak 250.

Oxygen Class Distribution. Figure 7 shows O_n class relative abundances for parent oak, oak 250, and oak 400. Oxygen classes for the parent material range from O_4 to O_{16}. The two

dx.doi.org/10.1021/ac202166x | Anal. Chem. 2012, 84, 1281−1287

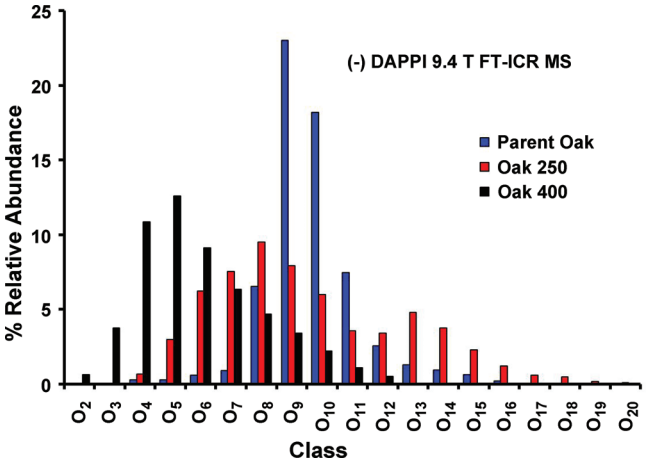

Figure 7. Percent relative abundance for various oxygen classes. Oak 250 has a bimodal distribution: formulas in the O_4–O_{11} classes are most likely thermally degraded lignin and cellulose compounds, whereas formulas in the O_{12}–O_{20} classes represent residual cellulose that is not thermally degraded and partially oxidized lignin and cellulose. Oak 400 formulas in the lower oxygen classes are the result of deacetylation caused by thermal degradation.

dominant oxygen classes are O_9 and O_{10}, with significant O_8 and O_{11} contributions. The narrow diversity in O_n classes is typical of fresh, labile biomass.

As for the DBE distribution, the O_n class distribution for oak 250 is bimodal, centered at ~O_8 and ~O_{13}. The bimodal distribution is consistent with the van Krevelen diagram for oak 250, in which compounds with distributions are centered at relatively low and high O/C and H/C. The relatively lower oxygen components may be attributed to dehydration of hemicellulose and lignin, beginning at ~200 °C.[59] The higher oxygen species (~O_{12}–O_{20}) may arise from partial oxidation of lignin due to incomplete combustion or thermally undegraded cellulose.

Additional evidence for deacetylation of hemicellulose is evidenced from the oxygen class graph for oak 400. The oxygen classes for oak 400 range from O_2 to O_{12}, centered at O_5. The lower oxygen numbers suggest that the lower O/C ratios observed in Figure 3 are likely due to a combination of deacetylation and dehydration. The net change in O/C ratio from deacetylation (loss of H_2CO) is negative (provided that, as in this case, there are more carbons than oxygens in the molecule), and the net change in O/C ratio is always negative for dehydration because one oxygen is lost, without the loss of carbons.

AUTHOR INFORMATION

Corresponding Author

*Phone: +1-850-644-6875. Fax: +1-850-644-8281. E-mail: cooper@chem.fsu.edu.

ACKNOWLEDGMENTS

We thank Dr. Andrew Zimmerman at the University of Florida for the char samples, Christopher Hendrickson, Nathan Kaiser, Joshua Savory, and John Paul Quinn for their constant updates to the 9.4 T FTICR mass spectrometer, and Greg Blakney for the development of the molecular formula calculator. This work was supported by the National Science Foundation (EAR-0628349 and DMR-06-54118) and the State of Florida.

REFERENCES

(1) ZiolkowskiL. A.DruffelE. R. M.Geophys. Res. Lett.2010, 10.1029/2010gl043963
(2) Bird, M. I.; Grocke, D. R. *Geochim. Cosmochim. Acta.* **1997**, *61*, 3413–3423.
(3) Cope, M. J.; Chaloner, W. G. *Nature* **1980**, *283*, 647–649.
(4) Glaser, B.; Haumaier, L.; Guggenberger, G.; Zech, W. *Naturwissenschaften* **2001**, *88*, 37–41.
(5) Seiler, W.; Crutzen, P. J. *Clim. Change* **1980**, *2*, 207–247.
(6) Crutzen, P. J.; Andreae, M. O. *Science* **1990**, *250*, 1669–1678.
(7) Kuhlbusch, T. A. J.; Crutzen, P. J. *Global Biogeochem. Cycles* **1995**, *9*, 491–501.
(8) Baldock, J. A.; Smernick, R. J. *Org. Geochem.* **2002**, *33*, 1093–1109.
(9) Goldberg, E. D. *Black Carbon in the Environment: Properties and Distribution*; John Wiley and Sons: New York, 1985.
(10) Hamer, U.; Marschner, B.; Brodowski, S.; Amelung, W. *Org. Geochem.* **2004**, *35*, 823–830.
(11) Shneour, E. A. *Science* **1966**, *151*, 991–992.
(12) Scott, C. D.; Strandberg, G. W.; Lewis, S. N. *Biotechnol. Prog.* **1986**, *2*, 131–139.
(13) Hofrichter, M.; Ziegenhagen, D.; Sorge, S.; Ullrich, R.; Bublitz, F.; Fritsche, W. *Appl. Microbiol. Biotechnol.* **1999**, *52*, 78–84.
(14) Bird, M. I.; Cali, J. A. *Nature* **1998**, *394*, 767–769.
(15) Bird, M. I.; Moyo, C.; Veenendaal, E. M.; Lloyd, J.; Frost, P. *Global Biogeochem. Cycles* **1999**, *13*, 923–932.
(16) Preston, C. M.; Schmidt, M. W. I. *Biogeosciences* **2006**, *3*, 397–420.
(17) Alexis, M. A.; Rumpel, C.; Knicker, H.; Leifeld, J.; Rasse, D.; Pechot, N.; Bardoux, G.; Mariotti, A. *Org. Geochem.* **2010**, *41*, 690–697.
(18) Nguyen, B. T.; Lehmann, J.; Hockaday, W. C.; Joseph, S.; Masiello, C. A. *Environ. Sci. Technol.* **2010**, *44*, 3324–3331.
(19) McBeath, A. V.; Smernick, R. J. *Org. Geochem.* **2009**, *40*, 1161–1168.
(20) Kujawinski, E. B.; Del Vecchio, R.; Blough, N. V.; Klein, G. C.; Marshall, A. G. *Mar. Chem.* **2004**, *92*, 23–37.
(21) Marshall, A. G.; Hendrickson, C. L.; Jackson, G. S. *Mass Spectrom. Rev.* **1998**, *17*, 1–35.
(22) Hockaday, W. C.; Grannas, A. M.; Kim, S. K.; Hatcher, P. G. *Org. Geochem.* **2006**, *37*, 501–510.
(23) Dittmar, T.; Koch, B. P. *Mar. Chem.* **2006**, *102*, 208–217.
(24) Kramer, R. W.; Kujawinski, E. B.; Hatcher, P. G. *Environ. Sci. Technol.* **2004**, *38*, 3387–3395.
(25) Stubbins, A.; Spencer, R. G. M.; Chen, H. M.; Hatcher, P. G.; Mopper, K.; Hernes, P. J.; Mwamba, V. L.; Mangangu, A. M.; Wabakanghanzi, J. N.; Six, J. *Limnol. Oceanogr.* **2010**, *55*, 1467–1477.
(26) Van Berkel, G. J.; Pasilis, S. P.; Ovchinnikova, O. *J. Mass Spectrom.* **2008**, *43*, 1161–1180.
(27) Chen, H.; Zheng, O. Y.; Cooks, R. G. *Angew. Chem., Int. Ed.* **2006**, *45*, 3656–3660.
(28) Coon, J. J.; McHale, K. J.; Harrison, W. W. *Rapid Commun. Mass Spectrom.* **2002**, *16*, 681–685.
(29) Shiea, J.; Huang, M. Z.; Hsu, H. J.; Lee, C. Y.; Yuan, C. H.; Beech, I.; Sunner, J. *Rapid Commun. Mass Spectrom.* **2005**, *19*, 3701–3704.
(30) Venter, A.; Nefliu, M.; Cooks, R. G. *TrAC, Trends Anal. Chem.* **2008**, *27*, 284–290.
(31) Takats, Z.; Wiseman, J. M.; Gologan, B.; Cooks, R. G. *Science* **2004**, *306*, 471–473.
(32) Cody, R. B.; Laramee, J. A.; Durst, H. D. *Anal. Chem.* **2005**, *77*, 2297–2302.
(33) Huang, M.-Z.; Yuan, C.-H.; Cheng, S.-C.; Cho, Y.-T.; Shiea, J. *Annu. Rev. Anal. Chem.* **2010**, *3*, 43–65.
(34) Robb, D. B.; Blades, M. W. *Anal. Chim. Acta* **2008**, *627*, 34–49.
(35) Haapala, M.; Pol, J.; Saarela, V.; Arvola, V.; Kotiaho, T.; Ketola, R. A.; Franssila, S.; Kauppila, T. J.; Kostiainen, R. *Anal. Chem.* **2007**, *79*, 7867–7872.

(36) Robb, D. B.; Covey, T. R.; Bruins, A. P. *Anal. Chem.* **2000**, *72*, 3653−3659.
(37) Hanold, K. A.; Fischer, S. M.; Cormia, P. H.; Miller, C. E.; Syage, J. A. *Anal. Chem.* **2004**, *76*, 2842−2851.
(38) Kauppila, T. J.; Arvola, V.; Haapala, M.; Pol, J.; Aalberg, L.; Saarela, V.; Franssila, S.; Kotiaho, T.; Kostiainen, R. *Rapid Commun. Mass Spectrom.* **2008**, *22*, 979−985.
(39) Luosujarvi, L.; Kanerva, S.; Saarela, V.; Franssila, S.; Kostiainen, R.; Kotiaho, T.; Kauppila, T. J. *Rapid Commun. Mass Spectrom.* **2010**, *24*, 1343−1350.
(40) Pol, J.; Vidova, V.; Kruppa, G.; Kobliha, V.; Novak, P.; Lemr, K.; Kotiaho, T.; Kostiainen, R.; Havlicek, V.; Volny, M. *Anal. Chem.* **2009**, *81*, 8479−8487.
(41) Purcell, J. M.; Hendrickson, C. L.; Rodgers, R. P.; Marshall, A. G. *Anal. Chem.* **2006**, *78*, 5906−5912.
(42) Kauppila, T. J.; Kotiaho, T.; Kostiainen, R.; Bruins, A. P. *J. Am. Soc. Mass Spectrom.* **2004**, *15*, 203−211.
(43) Kaiser, N. K.; Skulason, G. E.; Weisbrod, C. R.; Bruce, J. E. *J. Am. Soc. Mass Spectrom.* **2009**, *20*, 755−762.
(44) Blakney, G. T.; Hendrickson, C. L.; Marshall, A. G. *Int. J. Mass Spectrom.* **2011**, *306*, 346−252.
(45) Senko, M. W.; Hendrickson, C. L.; Emmett, M. R.; Shi, S. D.-H.; Marshall, A. G. *J. Am. Soc. Mass Spectrom.* **1997**, *8*, 970−976.
(46) Tolmachev, A. V.; Robinson, E. W.; Wu, S.; Kang, H.; Lourette, N. M.; Pasa-Tolic, L.; Smith, R. D. *J. Am. Soc. Mass Spectrom.* **2008**, *19*, 586−597.
(47) Kaiser, N. K.; Savory, J. J.; McKenna, A. M.; Quinn, J. P.; Hendrickson, C. L. *Anal. Chem.* **2011**, *83*, 6907−6910.
(48) Ledford, E. B. Jr.; Rempel, D. L.; Gross, M. L. *Anal. Chem.* **1984**, *56*, 2744−2748.
(49) Shi, S. D. H.; Drader, J. J.; Freitas, M. A.; Hendrickson, C. L.; Marshall, A. G. *Int. J. Mass Spectrom.* **2000**, *196*, 591−598.
(50) Kim, S.; Kramer, R. W.; Hatcher, P. G. *Anal. Chem.* **2003**, *75*, 5336−5344.
(51) Hammes, K.; Smernick, R. J.; Skjemstad, J. O.; Herzog, A.; Vogt, U. F.; Schmidt, M. W. I. *Org. Geochem.* **2006**, *37*, 1629−1633.
(52) Stenson, A. C.; Marshall, A. G.; Cooper, W. T. *Anal. Chem.* **2003**, *75*, 1275−1284.
(53) Hertkorn, N.; Benner, R.; Frommberger, M.; Schmitt-Kopplin, P.; Witt, M.; Kaiser, K.; Kettrup, A.; Hedges, J. I. *Geochim. Cosmochim. Acta* **2006**, *70*, 2990−3010.
(54) Glaser, B.; Lehmann, J.; Zech, W. *Biol. Fertil. Soils* **2002**, *35*, 219−230.
(55) Sjostrom, E. *Wood Chemistry. Fundamentals and Applications*, 2nd ed.; Academic Press: San Diego, 1993.
(56) Zhong, J.; Sleighter, R. L.; Salmon, E.; McKee, G. A.; Hatcher, P. G. *Org. Geochem.* **2011**, *42*, 903−916.
(57) Preston, C. M.; Trofymow, J. A.; Niu, J.; Fyfe, C. A. *Forest Ecol. Manage.* **1998**, *111*, 51−68.
(58) Shafizadeh, F. *Adv. Chem. Ser.* **1984**, *207*, 491−529.
(59) White, R. H.; Dietenberger, M. A. In *Encyclopedia of Materials: Science and Technology*; Buschow, K. H. J., Cahn, R. W., Flemings, M. C., Ilschner, B., Kramer, E. J., Mahajan, S., Veyssiere, P., Eds.; Elsevier: New York, 2001; pp 9712−9716.